### Title

Isomorphic Fluorescent Nucleosides Facilitate Real-Time Monitoring of RNA Depurination by Ribosome Inactivating Proteins




### Journal

Chemistry - A European Journal, 28(35)

### ISSN

0947-6539



### Authors

Cong, Deyuan
Li, Yao
Ludford, Paul T
et al.



### Publication Date

2022-06-21

### DOI

10.1002/chem.202200994

Peer reviewed

HHS Public Access

Author manuscript

*Chemistry*. Author manuscript; available in PMC 2023 June 21.

Published in final edited form as:

*Chemistry*. 2022 June 21; 28(35): e202200994. doi:10.1002/chem.202200994.

# Isomorphic Fluorescent Nucleosides Facilitate a Real-Time Monitoring of RNA Depurination by Ribosome Inactivating Proteins

**Deyuan Cong**,

**Yao Li**,

**Paul T. Ludford III**,

**Yitzhak Tor**

Department of Chemistry and Biochemistry, University of California, San Diego, 9500 Gilman Drive, La Jolla, CA 92093-0358 (USA)

## Abstract

Ribosome-inactivating proteins, a family of highly cytotoxic proteins, interfere with protein synthesis by depurinating a specific adenosine residue within the conserved α-sarcin/ricin loop of eukaryotic ribosomal RNA. Besides being biological warfare agents, certain RIPs have been promoted as potential therapeutic tools. Monitoring their deglycosylation activity and its inhibition in real time has remained, however, elusive. Herein, we describe the enzymatic preparation and utility of consensus RIP hairpin substrates in which specific G residues, neighboring the depurination site, are surgically replaced with $^{tz}$G and $^{th}$G, fluorescent G analogs. By strategically modifying key positions with responsive fluorescent surrogate nucleotides, RIP-mediated depurination can be monitored in real-time by steady state fluorescence spectroscopy. Subtle differences observed in preferential depurination sites provide insight into the RNA folding as well as RIPs' substrate recognition features.

## Graphical Abstract

**A real-time monitoring assay for RIP-mediated depurination**: Ribosome-inactivating proteins (RIPs) interfere with protein synthesis by depurinating a specific adenosine residue within α-sarcin/ricin loop. By strategically modifying key position with responsive fluorescent nucleosides such as $^{tz}$G, depurination by RIPs is monitored in real-time by fluorescence. The method provides insight into the RNA folding as well as RIPs' recognition features.

ytor@ucsd.edu .

Conflict of interest

The authors declare no conflict of interest

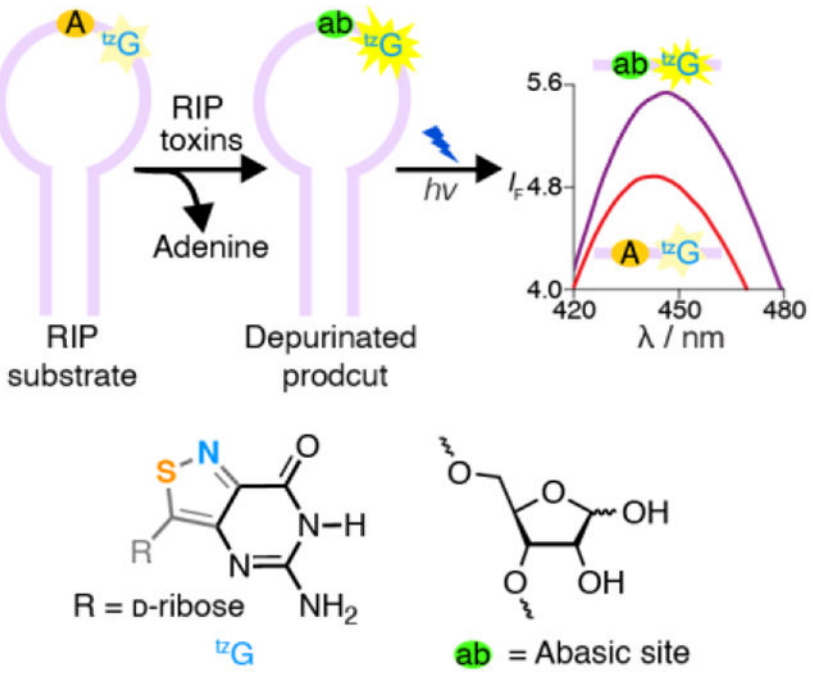


**Keywords**

fluorescence; RNA; protein toxins; emissive nucleosides; kinetics

Ribosome-inactivating proteins (RIPs), a family of highly toxic enzymes,[1] are broadly distributed among plants,[2] fungi[3] and bacteria[4] and have even been recently found in insects.[5] Their major catalytic depurinating activity leads to removal of a specific adenine from the α-sarcin-ricin loop,[6] a highly conserved ribosomal RNA domain, causing irreversible inhibition of protein synthesis.[7] While lethal to mammalian cells, RIPs can also display antiviral features[8] and can inhibit animal and plant viruses such as HIV-1,[9] poliovirus[10] and Tobacco etch virus.[11] RIP-conjugated toxins have also been developed as potential antitumor agents.[12,13] Their unique and surgically directed cellular activity, as well as potency and potential utility as biowarfare agents, have therefore attracted considerable interest over the years,[14] aiming particularly at the development of effective strategies for real time activity monitoring and detection.[15]

Prior studies have utilized Enzyme-linked immunosorbent assay (ELISA),[16] immuno-PCR[17] and mass spectrometry to assess RIP activity.[18] Most methods, however, require termination of the depurination reaction by either inactivating the enzyme or denaturating the RNA substrate. As such, these methods are not amenable to readily measure activity and its potential inhibition in real-time.

More than a decade ago we reported a fluorescence-based depurination-monitoring approach relying on $^{th}$U, an isomorphic responsive uridine analogue.[19] Incorporating this emissive U surrogate into an RNA oligonucleotide, complementary to the highly conserved α-sarcin-ricin loop, allowed us to simultaneously quench the RIP-mediated depurination reaction and

generate a fluorescent signal proportional to the reaction progress via enhanced emission (relying on the different emission intensity of $^{th}$U•A vs. $^{th}$U•A$_P$, due to their distinct microenvironments).[19] While powerful, this approach still fell short of the ultimate goal of monitoring RIP action in real time. The introduction of our highly isomorphic emissive RNA alphabets $^{th}$N and $^{tz}$N, based on thieno[3,4-*d*]pyrimidine[20] and isothiazolo[4,3-*d*]pyrimidine cores,[21] respectively, has made this previously unattainable task possible.

As *C*-nucleosides, the adenosine surrogates $^{th}$A and $^{tz}$A cannot replace the susceptible adenosine within the RNA substrate.[22] We hypothesized, however, that by placing the emissive and responsive $^{th}$G or $^{tz}$G either 5' or 3' to A$_{15}$, the depurinatable residue within the RNA substrate (Figure 1), activity would be maintained and fluorescence changes may be observed due to the environmental perturbations induced upon RIP-mediated generation of an abasic site. Inspecting the reported structures of the consensus RNA construct,[23] we hypothesized, however, that incorporation of fluorescent G surrogates 3' to the depurination site (i.e., at position 16), is likely to translate to a larger fluorescence signal upon depurination due to perturbation of the apparent A$_{15}$/G$_{16}$ stacking.[22] We further anticipated the $^{tz}$G-containing RNA substrates to perform better than their $^{th}$G counterparts due to the elevated isomorphicity of the former. Herein, we disclose the enzymatic synthesis of $^{th}$G- and $^{tz}$G-containing α-sarcin-ricin hairpin substrate RNAs and their RIP-mediated depurination reactions. We demonstrate that the emissive RNA substrates can be utilized to monitor enzymatic depurination in real-time. We critically assess the differences between the RNA substrates containing $^{tz}$G or $^{th}$G and compare the reaction kinetics and site preferences to that of a native RNA substrate.

The singly substituted RNA hairpin substrates **R1a** (Y=$^{tz}$G), **R1b (**Y=$^{th}$G**)** and **R2a** (Z=$^{tz}$G), containing the emissive guanosine surrogates at position G$_{16}$(Y)/G$_{14}$(Z) of the native substrate **R1** (Figure 1), were synthesized through $^{tz}$G/$^{th}$G-initiated transcription, followed by phosphorylation and ligation, using a general protocol we disclosed in 2017 (Figure 2a).[24] The T7 promoter and corresponding DNA template oligomers were annealed and transcribed in the presence of excess $^{tz}$G or $^{th}$G (as the free nucleosides) and natural NTPs (Figure 2b). The $^{tz}$G/$^{th}$G-containing transcripts **1a**/**1b** and unmodified native transcripts **1** were separated on a denaturing PAGE (Figure 2c, Figure S3, respectively). UV illumination (365 nm) visualized the desired and truncated RNA transcripts, which were analyzed by MALDI-TOF mass spectrometry (Figure 2c, 2d, Figure S2). Following a kinase-mediated 5'-phosphorylation and a T4 ligase-mediated ligation, the desired site specifically labeled fluorescent RNA constructs were separated by PAGE (Figure S3, Figure S5) and the isolated oligomers were subjected to MALDI and ESI mass spectrometry analyses (Figures S7-S14). To confirm the presence of intact $^{tz}$G or $^{th}$G and determine the ratio of each nucleoside, the RNA constructs were digested by S1 Nuclease, dephosphorylated and HPLC analyzed (Figure S15). The ratio of rC, rU, rA, rG, r$^{tz}$G/r$^{th}$G was 9.0:3.4:7.1:8.2:1 for $^{tz}$G modified strand **R1a**, and 11.2:4.5:9.2:7.7:1 for $^{th}$G modified strand **R1b**, respectively (r$^{tz}$G/r$^{th}$G was set as a reference value for calculation). The results were in reasonably good agreement with the expected theoretical ratio in **R1a**/**R1b** (rC, rU, rA, rG, r$^{tz}$G/r$^{th}$G is 9:3:7:9:1).

To categorically assess the viability of the modified RNAs as RIP substrates, the native and $^{tz}$G/$^{th}$G modified RNA substrates (**R1** and **R1a**/**R1b**, respectively) were subjected to

enzymatic depurination.[19] The hairpin RNA substrates, spiked with a trace amount of the corresponding $^{32}$P-labeled RNAs, were thermally denatured and refolded in a 30 mM Tris-HCl buffer. Depurination reactions with saporin as a representative RIP were carried out at 37 °C. Small aliquots of the reaction mixtures were treated with aniline-acetate buffer (pH 4.5) at given time intervals (to induce strand cleavage at the abasic sites)[25] and were resolved by PAGE (Figure 3a, 3b, 3c). T1 digestion and alkaline hydrolysis lanes reveal the sequence and assist in determining the cleavage site (Figure 3a, 3b, 3c: Lane T, A). As we previously demonstrated,[24] RNase T1, which is an N7-dependent ribonuclease, clearly shows the absence of a native G residue (and essentially a footprint) at the modification site (Figure 3b).

As seen in Figure 3, saporin largely depurinates the $A_{15}$ residue in the native and $^{tz}$G modified substrates (**R1** and **R1a**, respectively, Figure 3a, 3c) suggesting $^{tz}$G enables similar folding for **R1a** compared to **R1** and does not interfere with RIP activity. In contrast, the $^{th}$G substrate (**R1b**) is predominately depurinated at $A_9$, which appears to only be minimally/equally depurinated in the substrate **R1**/**R1a** (Figure 3b). Additionally, a similar depurination pattern was also observed for the emissive substrate **R2a** which is modified with $^{tz}$G at position 14 (Figure S17) indicating that $^{tz}G_{14}$ maintains similar folding compared to native **R1** substrate and does not interfere with saporin's recognition features. Additionally, longer reaction times were needed to completely consume **R1a** as well as **R2a** when compared to substrates **R1** and **R1b** (Figure 3d, S17). To quantify the observations, the apparent kinetic rate constants $k_{app}$, obtained by fitting pseudo-first order curves to the integrated PAGE bands plotted against time, were $2.14 \times 10^{-3}$, $0.48 \times 10^{-3}$ and $1.81 \times 10^{-3}$ $s^{-1}$ for substrate **R1**, **R1a**, and **R1b** respectively.

The observations reported above suggest a small perturbation in **R1a** when compared to the native substrate **R1**. As seen in the crystal structure of a bound cyclic tetranucleotide analogue of the RNA GAGA tetraloop, in which the susceptible adenosine has been replaced by 9-DA, a transition state analog (Figure 4a),[26] a cluster of aromatic residues including the RNA and two conserved tyrosine residues (Tyr73, Tyr123) forms. This unique cluster is further stabilized by an extensive hydrogen bonding network, which likely contributes to the depurination reaction. Substituting $G_{16}$ for $^{tz}$G in **R1a** might thus subtly perturb this intricate assembly, potentially lowering the population of catalytically active conformations, thus leading to its slightly slower depurination rate.

Intriguingly, when compared with **R1** and **R1a**, the $^{th}$G-containing **R1b** hairpin substrate showed a different reactivity pattern, with depurination predominantly at $A_9$ rather than $A_{15}$ (Figure 3b). This suggests that $^{th}$G's lower isomorphicity and G "mimicry", when compared to $^{tz}$G, particularly the lack of the basic N in the "N7" position, likely impacts the RNA substrate folding and recognition and thus the saporin-mediated depurination. As seen in the structure of the GAGA tetraloop (Figure 4b), the 2'-OH of $G_{14}$ H-bonds to N7 of $G_{16}$ (the residue replaced by either $^{tz}$G or $^{th}$G in the modified hairpin RNA strands **R1a** and **R1b**, respectively).[23] This missing attractive H bonding in the $^{th}$G-containing hairpin RNA, coupled to the potentially repulsive OH•••HC interaction, might impact the substrate folding, leading to non-specific depurination that has previously been proposed.[27]

Having established the viability of **R1a** and **R1b** as RIP substrates, their photophysical response upon enzymatic depurination with saporin was monitored by steady-state fluorescence spectroscopy under the same reaction conditions as for the radiolabeled constructs. Emission spectra were recorded at given time intervals as shown in Figure 5. For the $^{tz}$G substrate **R1a**, a noticeable decrease in fluorescence intensity was observed in the first 5 minutes, which was followed by steady increase as the reaction progressed. In contrast, a continuous fluorescence signal decrease was observed for the $^{th}$G modified substrate **R1b** upon exposure to saporin (Figure 5b). As anticipated, while a noticeable fluorescence decrease was observed for **R2a** in the first 5 minutes (likely reflecting folding/binding) there was no significant fluorescence intensity change following the reaction progress (Figure S18).

To aid in interpreting these observations and to confirm that the fluorescence-monitored data represents the same molecular event as visualized using the corresponding radiolabeled substrates, the data sets were normalized and depicted on the same graph (Figure 5c, 5d). The apparent kinetic rate constants $k_{app}$, obtained by fitting pseudo-first order curves to the integrated area of each spectrum plotted against time, yielded values of $0.51 \times 10^{-3}$ and $1.60 \times 10^{-3}$ $s^{-1}$ for substrate **R1a**, and **R1b** respectively (Figure 5c, 5d, Table 1). Notably, the apparent reaction rates generated by fluorescence for both **R1a** and **R1b** were in good agreement with the values extracted from the reactions visualized with the $^{32}$P-labeled substrates (Table 1), indicating the two techniques reflect the same molecular process and suggesting that fluorescence can indeed facilitate real-time monitoring of RIP-mediated RNA depurination.

Interpreting the specific fluorescence signal changes is, as always, more challenging as the trends observed reflect the collective influence of dynamically interacting and not necessarily orthogonal microenvironmental perturbations. For **R1a**, a rapid drop in fluorescence was followed by a slow steady increase, which nicely correlated with the reaction kinetics as determined by the radiolabeled substrate. The early fluorescence drop observed for **R1a** likely reflects a substrate/enzyme binding event, which alters the folding and likely places the emissive nucleobase in a desolvated pocket (Figure 4a). Since the adenine at $A_{15}$ stacks upon $^{tz}$G at the $G_{16}$ position (Figure 4b), its clipping generates a solvated and likely more polar void, which based upon the established photophysics of $^{tz}$G should lead to higher emission quantum yield and a slight bathochromic shift,[20] as observed.

For **R1b**, which predominantly depurinates at $A_9$, a decrease in fluorescence is seen. Since $^{th}G_{16}$ is not adjacent to the main depurination site, its photophysical change likely reflects a global conformational change of the depurinated RNA product. Since the $A_9$–$A_{21}$ pair lies between the Watson-Crick stem and the cross-strand stack (Figure 4c),[23] the lost hydrogen bond upon depurination of $A_9$ disrupts this non-canonical pair, which likely results in partial collapse of the GAGA tetraloop. This thus alters the microenvironment of $^{th}G_{16}$ and its dynamics, leading to a change in its fluorescence.[28]

**R2a**, containing a $^{tz}$G residue at position 14, undergoes enzymatic depurination (as independently established using PAGE, Figure S17). This, however, is not translated to

fluorescence changes that follow the reaction kinetics beyond the initial drop, attributed to binding and refolding. Inspection of the structure shown in Figure 4b suggests that depurination of $A_{15}$ is expected to be less environmentally perturbing (as it remains partially sandwiched between $G_{16}$ and $A_{17}$) when compared to the alteration of the stacked $A_{15}/G_{16}$ pair as in **R1a**, as hypothesized.

In summary, $^{th}$G and $^{tz}$G, highly isomorphic fluorescent nucleoside surrogates, are found to be accepted by several enzymes including T7 polymerase, T4 kinase and T4 ligase, allowing one to easily fabricate singly-substituted emissive RNA constructs. To advance the long sought-after direct monitoring of RNA depurination, we applied this protocol for the enzymatic preparation of consensus RIP hairpin substrates in which specific G residues, neighboring the depurination site, have been strategically replaced with these two emissive G surrogates. We demonstrated these enzymatic depurination reactions could indeed be monitored in real-time by steady state fluorescence spectroscopy. This unprecedented observation stands in contrast to other reported RIP-detecting methods, which all include either stepwise or time-consuming indirect processes (e.g., PCR-based techniques,[29] RNA/DNA probe hybridization,[19,30,31] aptamer-based,[32] enzyme-coupled assays,[15,33] mass spectrometry,[34] electrochemistry,[35] etc.). Monitoring a specific biochemical transformation associated with such RNA toxins (i.e., depurination), regardless of the protein immunological fingerprint, thus facilitates pathways for real-time detection of such cytotoxins and the fabrication of inhibitor discovery tools.

## Supplementary Material

Refer to Web version on PubMed Central for supplementary material.

## Acknowledgements

We thank the National Institutes of Health for generous support (through grant GM 139407) and the UCSD Chemistry and Biochemistry MS Facility.

## References

[1]. Sturm MB, Roday S, Schramm VL, J. Am. Chem. Soc 2007, 129, 5544–5550. [PubMed: 17417841]

[2]. Law SK-Y, Wang R-R, Mak AN-S, Wong K-B, Zheng Y-T, Shaw P-C, Nucleic Acids Res. 2010, 38, 6803–6812. [PubMed: 20558598]

[3]. Chan WY, Ng TB, Lam JSY, Wong JH, Chu KT, Ngai PHK, Lam SK, Wang HX, Appl. Microbiol. Biotechnol 2010, 85, 985–993. [PubMed: 19568748]

[4]. Chan YS, Ng TB, Appl. Microbiol. Biotechnol 2016, 100, 1597–1610. [PubMed: 26685676]

[5]. Lapadula WJ, Marcet PL, Mascotti ML, Sanchez-Puerta MV, Juri Ayub M, Sci. Rep 2017, 7, 1863. [PubMed: 28500327]

[6]. Irvin JD, Uckun FM, Pharmacol. Ther 1992, 55, 279–302. [PubMed: 1492120]

[7]. Lord JM, Roberts LM, Robertus JD, FASEB J. 1994, 8, 201–208. [PubMed: 8119491]

[8]. Domashevskiy AV, Goss DJ, Toxins 2015, 7, 274–298. [PubMed: 25635465]

[9]. a)Lu J-Q, Zhu Z-N, Zheng Y-T, Shaw P-C, Toxins 2020, 12, 167;b)Zarling JM, Moran PA, Haffar O, Sias J, Richman DD, Spina CA, Myers DE, Kuebelbeck V, Ledbetter JA, Uckun FM, Nature 1990, 347, 92–95.

[10]. Cardinali B, Fiore L, Campioni N, De Dominicis A, Pierandrei-Amaldi P, J. Virol 1999, 73, 7070–7076. [PubMed: 10400812]

[11]. Domashevskiy AV, Williams S, Kluge C, Cheng S-Y, Biochemistry 2017, 56, 5980–5990. [PubMed: 29064680]

[12]. Sun W, Sun J, Zhang H, Meng Y, Li L, Li G, Zhang X, Meng Y, Sci. Rep 2018, 8, 17729. [PubMed: 30531997]

[13]. a)Polito L, Bortolotti M, Mercatelli D, Battelli MG, Bolognesi A, Toxins 2013, 5, 1698–1722; [PubMed: 24105401] b)Yuan H, Stratton CF, Schramm VL, ACS Chem. Biol 2016, 11, 1383–1390. [PubMed: 26886255]

[14]. a)Puri M, Kaur I, Perugini MA, Gupta RC, Drug Discovery Today 2012, 17, 774–783; [PubMed: 22484096] b)Walper SA, Lasarte Aragonés G, Sapsford KE, Brown CW, Rowland CE, Breger JC, Medintz IL, ACS Sens. 2018, 3, 1894–2024. [PubMed: 30080029]

[15]. Sturm MB, Schramm VL, Anal. Chem 2009, 81, 2847–2853. [PubMed: 19364139]

[16]. Guo J, Shen B, Sun Y, Yu M, Hu M, Hybridoma (Larchmt) 2006, 25, 225–229. [PubMed: 16934019]

[17]. He X, McMahon S, McKeon TA, Brandon DL, J. Food Prot 2010, 73, 695–700. [PubMed: 20377958]

[18]. Kull S, Pauly D, Störmann B, Kirchner S, Stämmler M, Dorner MB, Lasch P, Naumann D, Dorner BG, Anal. Chem 2010, 82, 2916–2924. [PubMed: 20199054]

[19]. Srivatsan SG, Greco NJ, Tor Y, Angew. Chem. Int. Ed 2008, 47, 6661–6665.Angew. Chem 2008, 120, 6763–6767.

[20]. Rovira AR, Fin A, Tor Y, J. Am. Chem. Soc 2015, 137, 14602–14605. [PubMed: 26523462]

[21]. Shin D, Sinkeldam RW, Tor Y, J. Am. Chem. Soc 2011, 133, 14912–14915. [PubMed: 21866967]

[22]. Tanaka KSE, Chen X-Y, Ichikawa Y, Tyler PC, Furneaux RH, Schramm VL, Biochemistry 2001, 40, 6845–6851. [PubMed: 11389598]

[23]. Correll CC, Munishkin A, Chan YL, Ren Z, Wool IG, Steitz TA, Proc. Natl. Acad. Sci. U. S. A 1998, 95, 13436–13441. [PubMed: 9811818]

[24]. Li Y, Fin A, McCoy L, Tor Y, Angew. Chem. Int. Ed 2017, 56, 1303–1307.Angew. Chem 2017, 129, 1323–1327.

[25]. Küpfer PA, Leumann CJ, Nucleic Acids Res. 2007, 35, 58–68. [PubMed: 17151071]

[26]. Ho MC, Sturm MB, Almo SC, Schramm VL, Proc. Natl. Acad. Sci. U. S. A 2009, 106, 20276–20281. [PubMed: 19920175]

[27]. Tan Q-Q, Dong D-X, Yin X-W, Sun J, Ren H-J, Li R-X, J. Biotechnol 2009, 139, 156–162. [PubMed: 19014981]

[28]. Kuchlyan J, Martinez-Fernandez L, Mori M, Gavvala K, Ciaco S, Boudier C, Richert L, Didier P, Tor Y, Improta R, Mély Y, J. Am. Chem. Soc 2020, 142, 16999–17014. [PubMed: 32915558]

[29]. Melchior WB, Tollenson WH, Anal. Biochem 2010, 396, 204–211. [PubMed: 19766090]

[30]. Tanpure AA, Srivatsan SG, ChemBioChem. 2012, 13, 2392–2399. [PubMed: 23070860]

[31]. Tanpure AA, Patheja P, Srivatsan SG, Chem Commun. 2012, 48, 501–503.

[32]. Esteban-Fernández de Ávila B, Lopez-Ramirez MA, Báez DF, Jodra A, Singh VV, Kaufmann K, Wang J, ACS Sens. 2016, 1, 217–221.

[33]. Mei Q, Fredrickson CK, Lian W, Jin S, Fan ZH, Anal. Chem 2006, 78, 7659–7664. [PubMed: 17105156]

[34]. Bevilacqua VLH, Nilles JM, Rice JS, Connell TR, Schenning AM, Reilly LM, Durst HD, Anal. Chem 2010, 82, 798–800. [PubMed: 20055481]

[35]. Oliveira G, Schneedorf JM, Toxins 2021, 13, 238 [PubMed: 33810228]

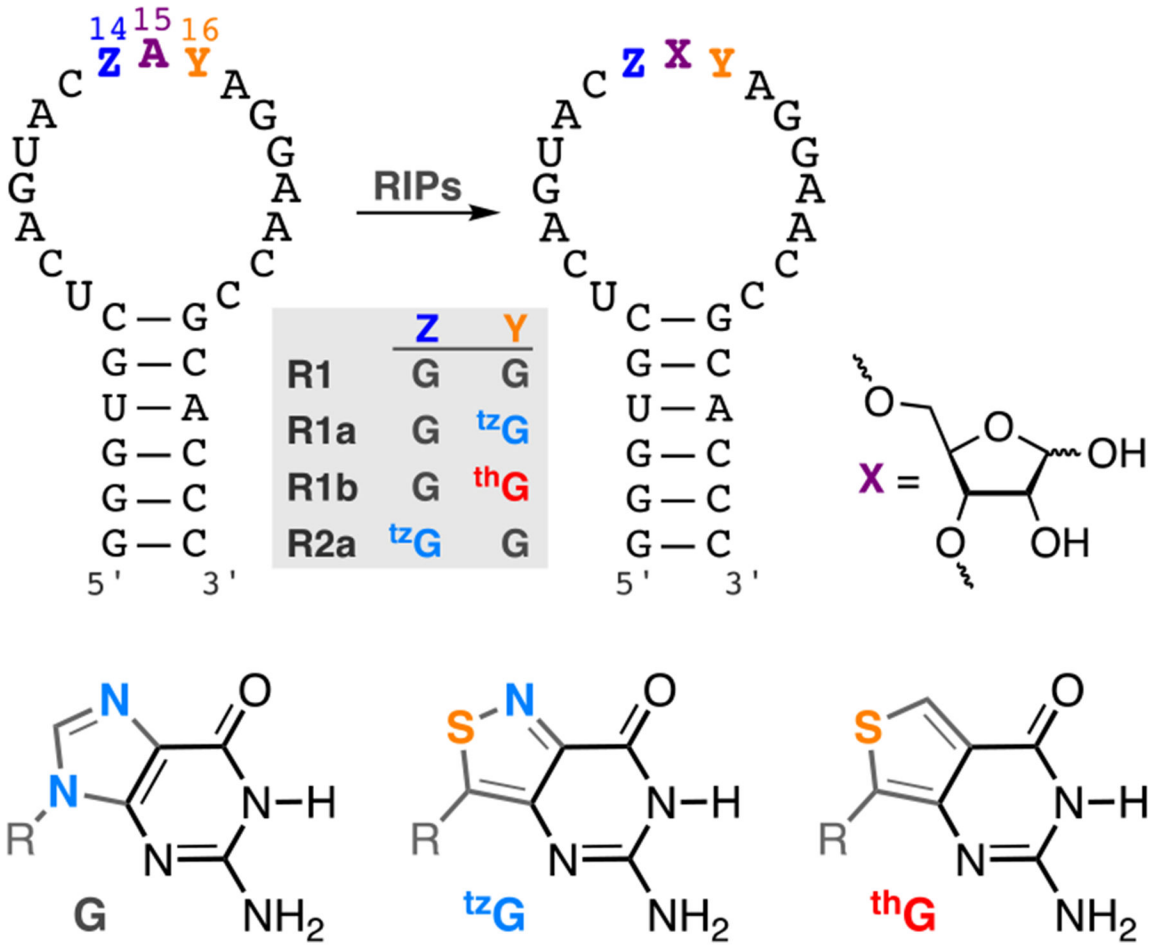


**Figure 1.**

RIP-mediated depurination of $A_{15}$ in the α-sarcin/ricin loop RNA substrate yields an abasic site. **R1**, **R1a**, **R1b, R2a** are the native, $^{tz}G_{16}$, $^{th}G_{16}$, and $^{tz}G_{14}$ modified hairpin substrates, respectively. R = D-ribose

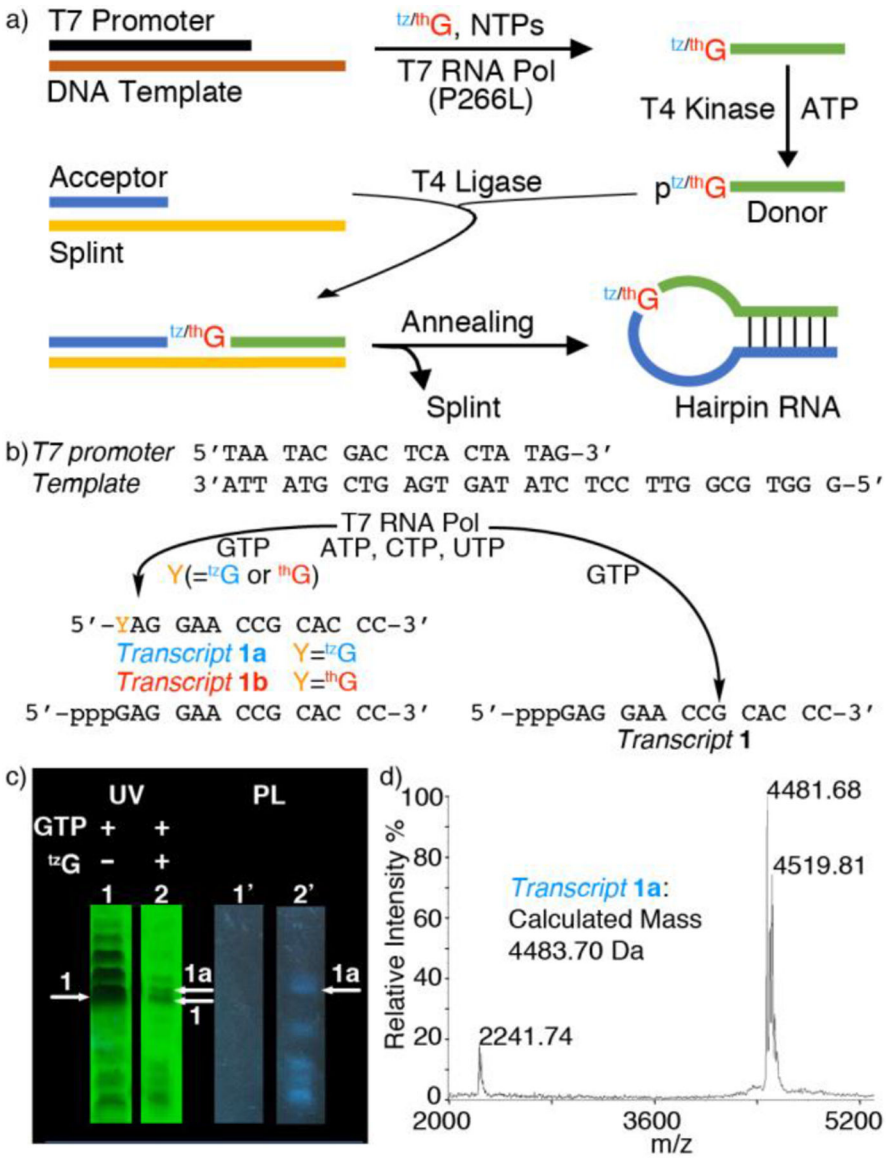


**Figure 2.**

a) Enzymatic pathways to singly modified hairpin RNAs via transcription, phosphorylation and ligation, replacing a single native guanosine with $^{th}$G or $^{tz}$G. See reference 24 for details of the general approach. b) Transcription reactions in the presence of natural NTPs using the T7 promotor and template shown, with or without $^{tz}$G/$^{th}$G. c) PAGE analysis of transcription reactions using 2 mM NTPs with or without 10 mM $^{tz}$G. Lane 1 and 1': native transcription without $^{tz}$G. Lane 2 and 2': transcription with 10 mM $^{tz}$G. White arrows indicated the expected product transcript **1a** (arrow 1a) and transcript **1** (arrow 1). UV: UV shadowing upon illumination at 254 nm; PL: photoluminescence upon excitation at 365 nm; d) MALDI MS of transcript **1a**.

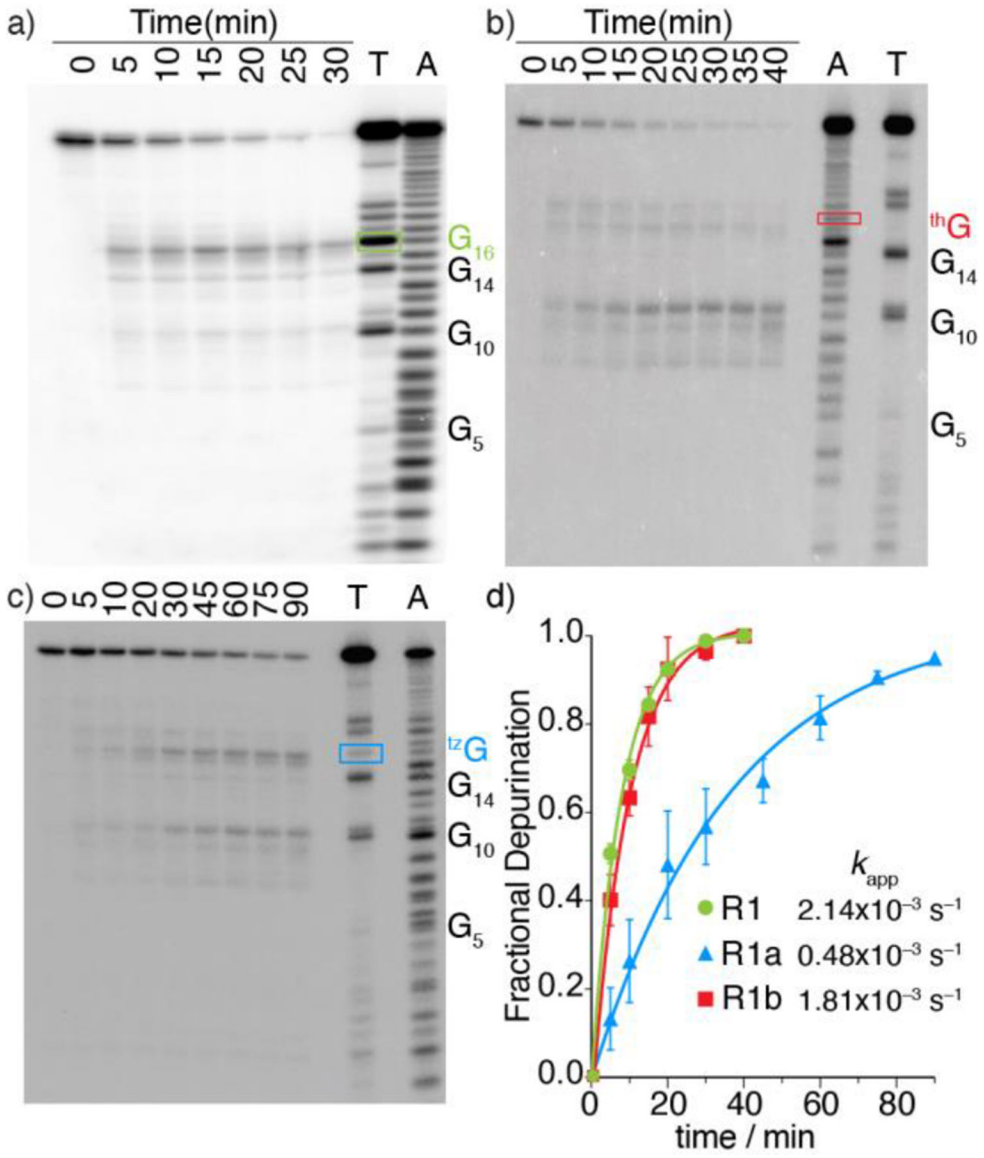


**Figure 3.**

Saporin-mediated depurination of native and $^{tz}$G/$^{th}$G-modified RNA substrates (**R1** and **R1a**/**R1b**, respectively) spiked with the corresponding $^{32}$P-labeled constructs and resolved by 20% PAGE. All reactions were carried out in Tris buffer (30 mM, pH 6.0), NaCl (25 mM) and $MgCl_2$ (2 mM) at 37 °C. All lanes were treated with aniline-acetate buffer (pH 4.5) at the indicated time intervals. Lanes T and A correspond to RNase T1 digestion and alkaline hydrolysis ladder, respectively. The bands labeled by rectangles in a, b and c, indicate the modified site with native G, $^{th}$G, and $^{tz}$G at $G_{16}$ position, respectively. a) Depurination reaction of **R1**. b) Depurination reaction of **R1b**. The missing band from lane T of **R1b** indicated a footprint at position $G_{16}$, which is replaced by $^{th}$G. c) Depurination reaction of **R1a** at given time point. d) Kinetic profiles of saporin-mediated depurination reactions of $^{32}$P-5'-labeled **R1** (Green), **R1a** (Blue) and **R1b** (Red). Reactions were done in triplicates and a representative gel is shown per experiment. Error bars indicate SD.

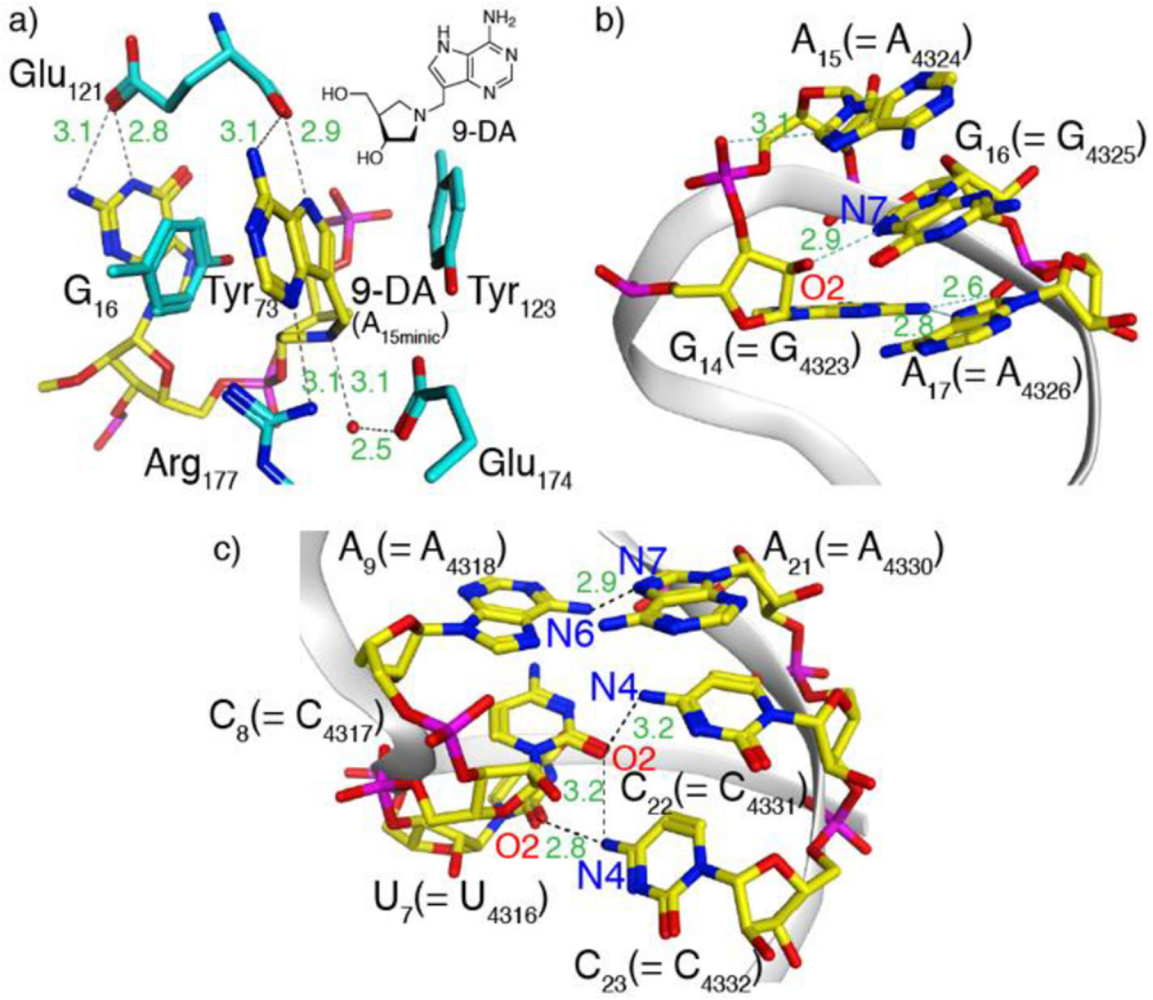


**Figure 4.**

a) Aromatic–aromatic interactions in saporin's active site when bound to a cyclic tetranucleotide analogue of the RNA GAGA tetraloop, in which the susceptible adenosine has been replaced by 9-DA, a transition state analogue, illustrating the interaction between the latter and two tyrosine residues (PDB ID code 3HIW).[26] Nucleosides are shown in yellow and the amino acid side chains are shown in cyan. Inset: the structure of 9-DA. Generic numbering is shown as absolute numbering changes between species; $A_{15}$ = $A_{4324}$ in the rat 28S rRNA numbering. b) X-ray structure of the α-sarcin-ricin loop highlighting the GAGA tetraloop and its aromatic–aromatic interactions. c) X-ray structure of the α-sarcin-ricin loop highlighting $A_9$–$A_{21}$ and adjacent base pairs in the stem (PDB ID code 430D for b,c).[23] Images generated using MOE.

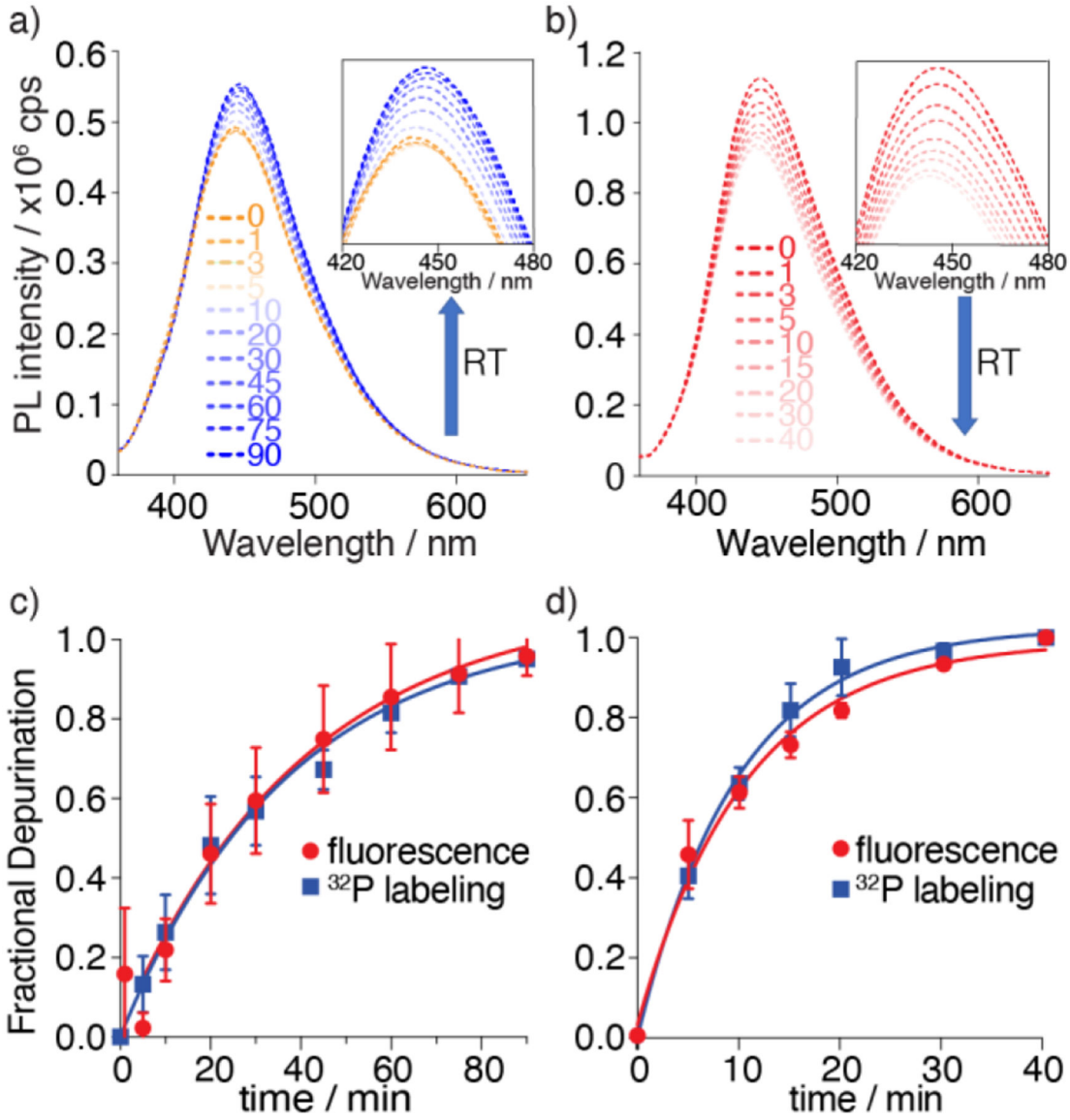


**Figure 5.**

Top: Saporin-mediated depurination reaction of substrate **R1a** and **R1b** monitored by fluorescence as function of reaction time (RT), respectively. a) Emission spectra of depurination reaction of $^{tz}$G substrate **R1a**. Excitation wavelength was 351 nm. Inset: Emission from 420 to 480 nm b) Emission spectra of depurination reaction of $^{th}$G substrate **R1b**. Excitation wavelength was 351 nm. Inset: Emission from 420 to 480 nm. The area of each spectrum was integrated and plotted vs. time to yield the kinetics of the enzymatic reaction (c,d). c) Fractional depurination of **R1a** by saporin at various time points monitored by fluorescence (red) and $^{32}$P radiolabeling (blue). d) Fractional depurination of **R1b** by saporin at various time points monitored by fluorescence (red) and $^{32}$P radiolabeling (blue). Assays were done in triplicates. Error bars indicate SD.

**Table 1.**

Reaction rate constants for saporin mediated depurination.

| | $^{32}$P-labeling[a] | | | Fluorescence[b] | |
|---|---|---|---|---|---|
| | **R1** | **R1a** | **R1b** | **R1a** | **R1b** |
| $k_{app}$ [c] | 2.14 ± 0.07 | 0.48 ± 0.02 | 1.81± 0.06 | 0.51 ± 0.02 | 1.60 ± 0.08 |
| $t_{1/2}$ [d] | 3.24 ± 0.10 | 14.4 ± 0.5 | 3.84 ± 0.14 | 13.9 ± 0.5 | 4.36 ± 0.24 |
| $R^2$ | 0.998 | 0.996 | 0.998 | 0.994 | 0.994 |

[a] Reaction rate constants were obtained by depurination reaction of $^{32}$P-5'-labeled substrate **R1**, **R1a** and **R1b.**

[b] Reaction rate constants were obtained by measuring fluorescence change.

[c] $k_{app}$ is the pseudo-first-order rate constant [x$10^{-3}$ $s^{-1}$].

[d] $t_{1/2}$ is half-life [x$10^2$ s]. Data are presented as mean ± SD.